Supporting Information S1

Diffuse reflectance spectra and Tauc plots for the initial protonated titanates

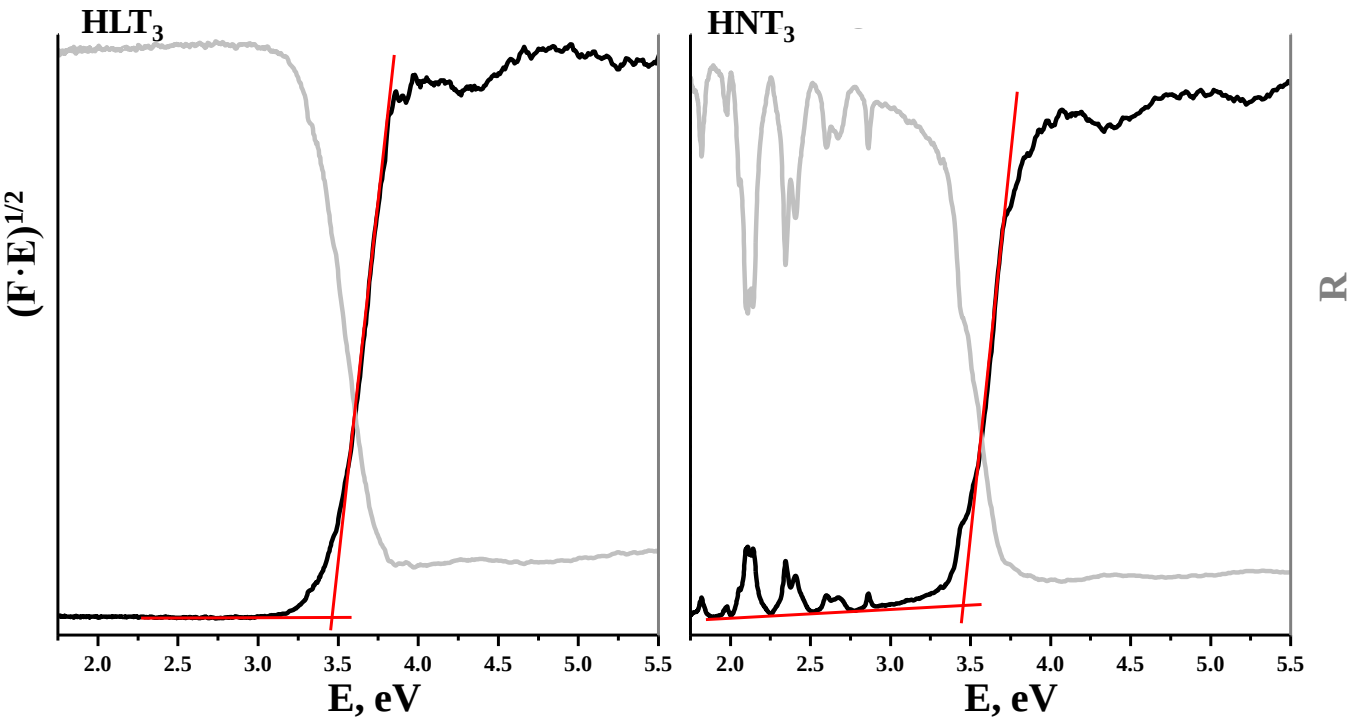

Supporting Information S2

Diffuse reflectance spectra and Tauc plots for inorganic-organic derivatives

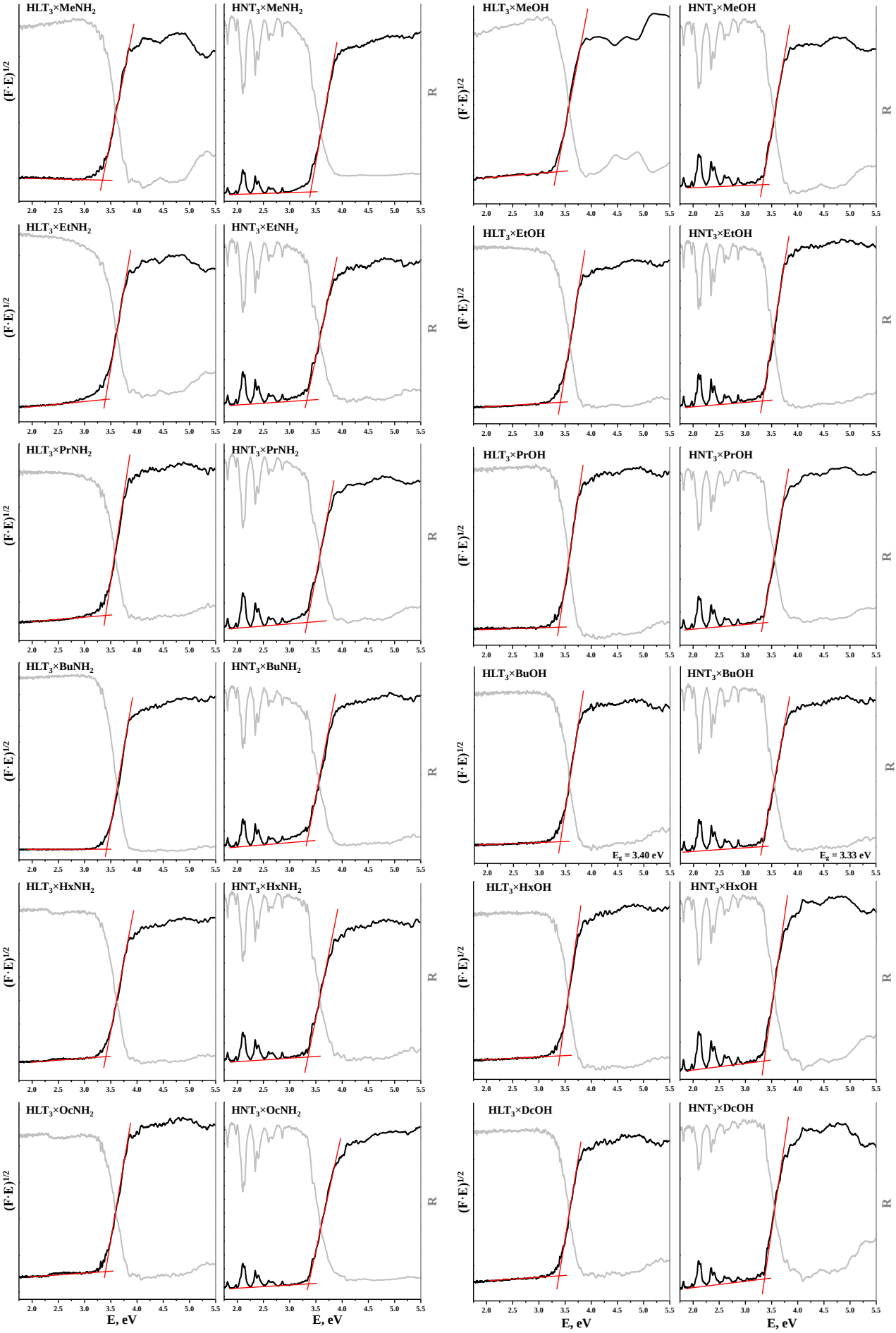

Supporting Information S3

SEM images of HLT_3 and its inorganic-organic derivatives

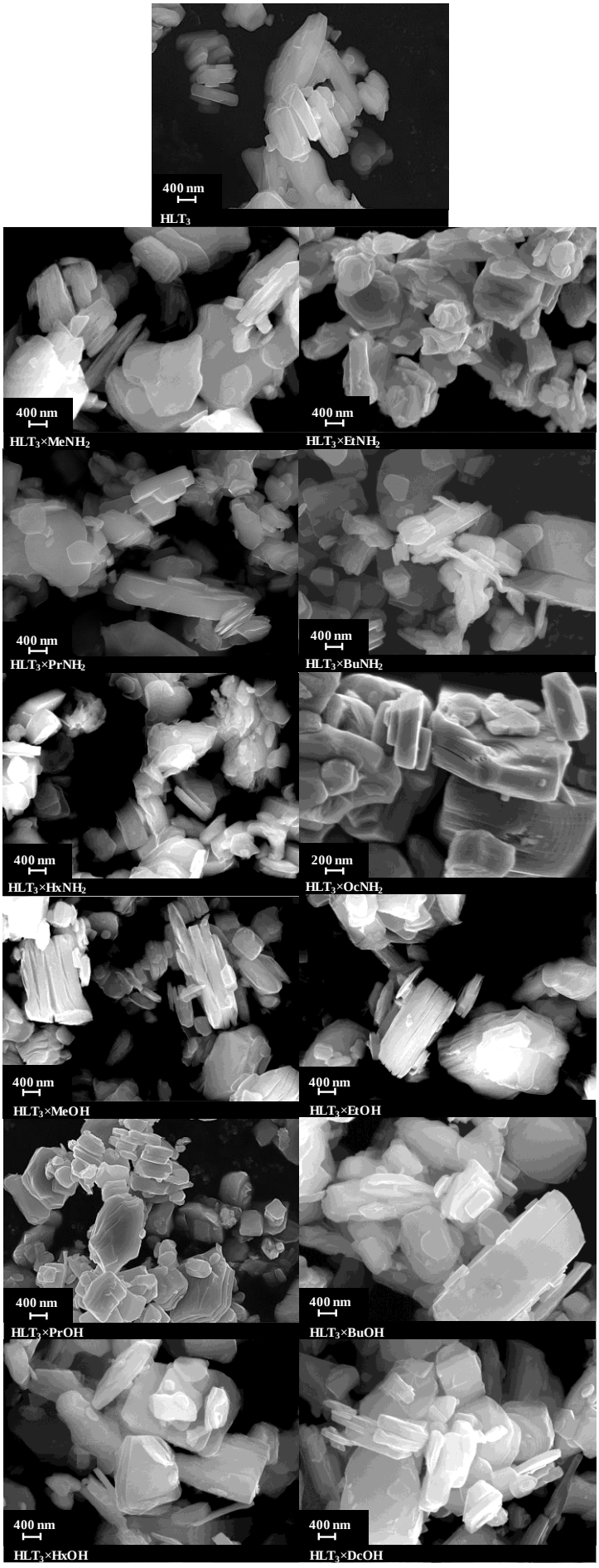

Supporting Information S4

SEM images of HNT_3 and its inorganic-organic derivatives

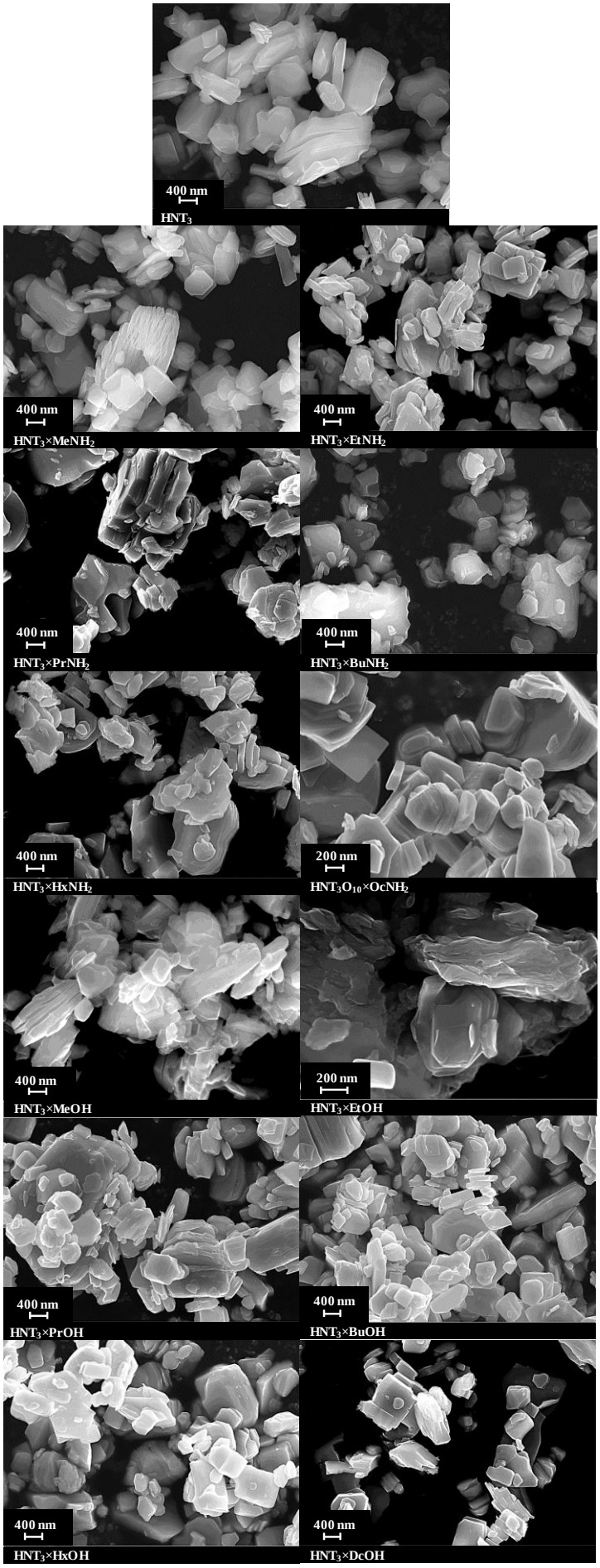

Supporting Information S5

TG analysis of the initial protonated titanates and their inorganic-organic derivatives

TG curves of the protonated precursors and hybrid compounds shown below were recorded in an oxidative atmosphere. Thermal degradation of the protonated samples includes two stages. The first of them relates to the temperatures below 275°C and corresponds to deintercalation of interlayer water with the formation of the anhydrous titanate. The second one (275–450°C) is referred to topochemical condensation of the latter, which is known to consist in combining of interlayer oxygen anions and protons in water molecules whose liberation is followed by closing adjacent perovskite blocks. Thus, the final products of thermolysis can be described by gross formulae $Ln_2Ti_3O_9$. Thermal degradation of the hybrid inorganic-organic compounds represents a more complex process. Based on the behavior of their TG curves and the data of the simultaneous thermal analysis coupled with mass spectroscopy (STA-mass) presented for the kindred Ruddlesden-Popper titanates in our previous reports, the following thermolysis mechanism can be suggested. Decomposition of the *n*-alkylamine compounds starts with evolution of interlayer water and amine molecules proceeding in the range of 50–250°C. Their joint liberation, apparently associated with strong hydrogen bonding, makes it impossible to separate mass loss values caused by to the removal of each of the interlayer components. The subsequent course of the curves shows that the *n*-alkylamine deintercalation does not occur fully and its completeness declines with growing of the amine chain length. In the temperature range of 275–450°C, topochemical dehydration of the protonated titanate matrix and, potentially, partial decay of the residual *n*-alkylamine occur. The subsequent thermolysis stage (450–600°C) is characterized by the mass gain explained by partial oxidation of the carbon-containing interlayer component. TG data do not allow rigorously establishing the specific form the carbon existence under these conditions. Further heating (600–900°C) results in its complete oxidation to carbon dioxide, which provides the corresponding mass loss and the plateau curve output referred to the mass of the solid inorganic residue. The initial section on the curves of the *n*-alkoxy compounds (50–250°C) relates to interlayer water deintercalation; in the case of the *n*-decoxy compounds, it might be also referred to residual *n*-heptane liberation, which served as a solvent during synthesis. Heating up to 300–350°C is accompanied by partial degradation of *n*-alkoxy groups and topochemical condensation of the titanate via the free vertices of interlayer titanium-oxygen octahedra. Subsequent heating (400–650°C) provides the pronounced mass gain because of the partial oxidation of the residual carbon-containing component, whose main part appears to preserve in the sample at the beginning of this section. In the high temperature region (650–900°C), like in the case of the *n*-alkylamine compounds, the carbon residue completely burns out forming carbon dioxide. However, liberation of molecular alcohols does not take place at any stage of thermolysis, which consists with covalent nature of the *n*-alkoxy derivatives.

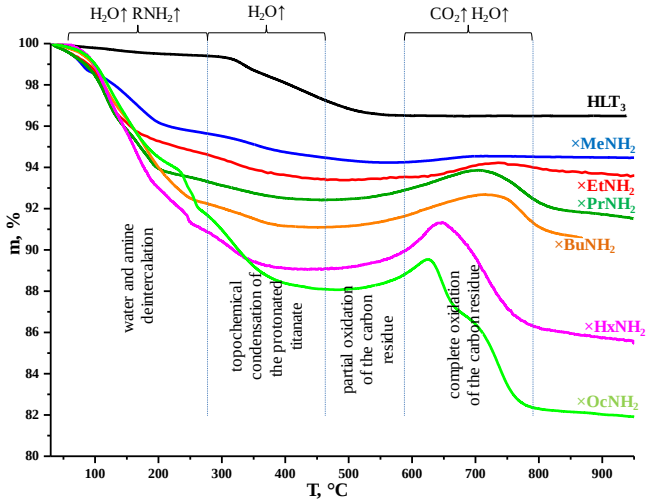
H2O↑ RNH2↑
H2O↑
CO2↑ H2O↑
HLT3
×MeNH2
×EtNH2
×PrNH2
×BuNH2
×HxNH2
×OcNH2
water and amine deintercalation
topochemical condensation of the protonated titanate
partial oxidation of the carbon residue
complete oxidation of the carbon residue
m, %
T, °C

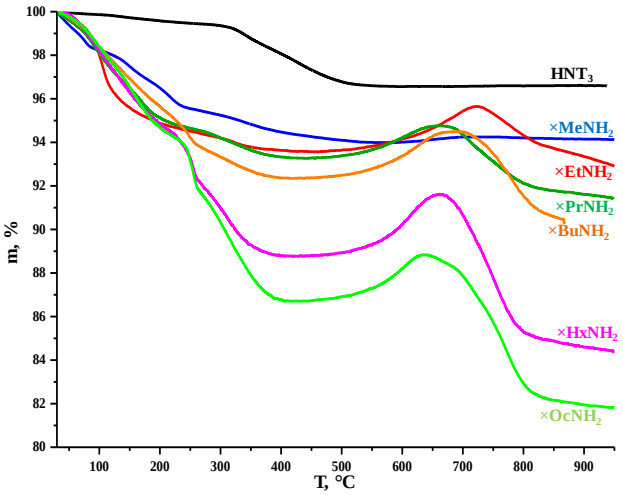
HNT3
×MeNH2
×EtNH2
×PrNH2
×BuNH2
×HxNH2
×OcNH2
m, %
T, °C

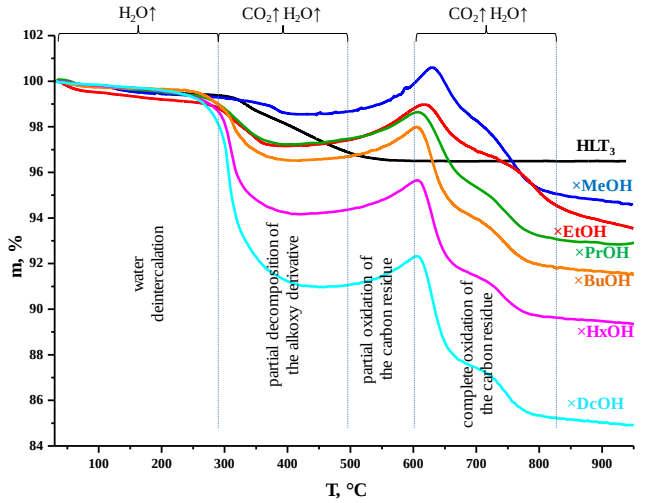
H2O↑
CO2↑ H2O↑
CO2↑ H2O↑
HLT3
×MeOH
×EtOH
×PrOH
×BuOH
×HxOH
×DcOH
water deintercalation
partial decomposition of the alkoxy derivative
partial oxidation of the carbon residue
complete oxidation of the carbon residue
m, %
T, °C

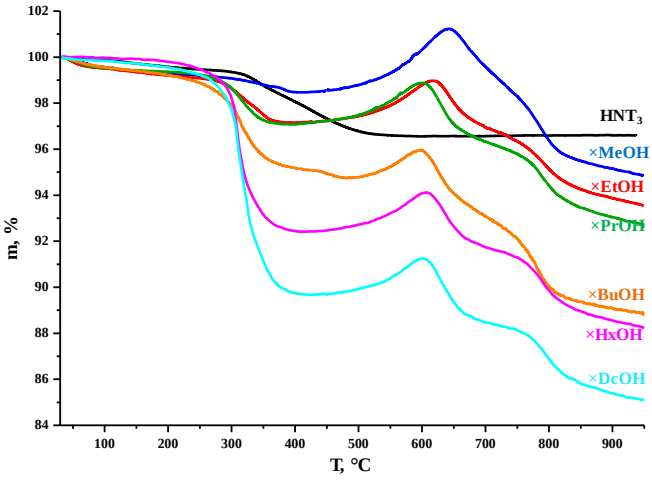
HNT3
×MeOH
×EtOH
×PrOH
×BuOH
×HxOH
×DcOH
m, %
T, °C

Supporting Information S6

Data on vacuum stability of inorganic-organic derivatives

Sample	Total mass loss, %	
	5 d vacuum	10 d vacuum
$HLT_3 \times MeNH_2$	2.82	2.85
$HNT_3 \times MeNH_2$	2.76	2.78
$HLT_3 \times BuNH_2$	2.26	2.28
$HNT_3 \times BuNH_2$	2.09	2.12
$HLT_3 \times OcNH_2$	1.04	1.04
$HNT_3 \times OcNH_2$	1.02	1.02
$HLT_3 \times MeOH$	0.00	0.00
$HNT_3 \times MeOH$	0.17	0.18
$HLT_3 \times BuOH$	0.65	0.66
$HNT_3 \times BuOH$	0.57	0.57
$HLT_3 \times DcOH$	0.49	0.49
$HNT_3 \times DcOH$	0.43	0.43

Supporting Information S7

Raman spectra of some inorganic-organic derivatives before and after 10 d keeping under vacuum

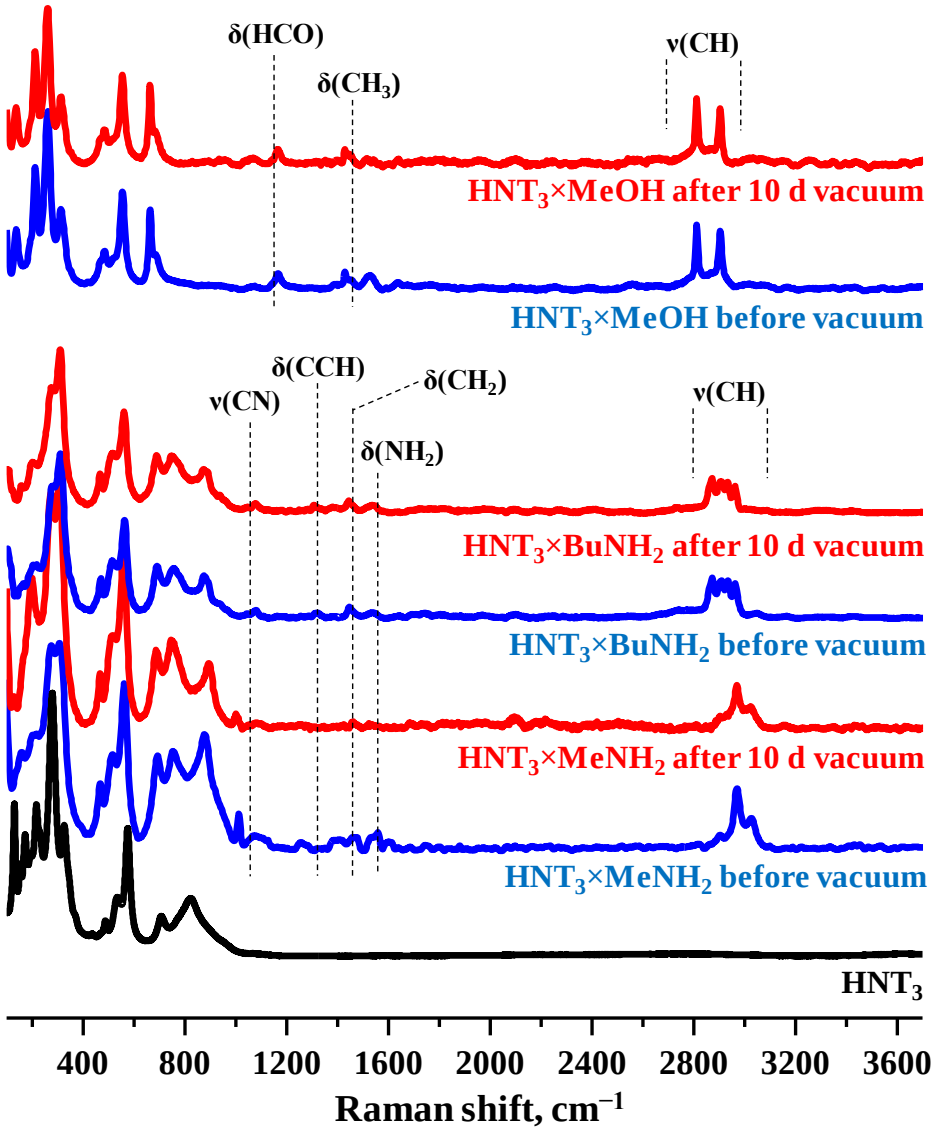

Supporting Information S8

XRD patterns of Nd-containing inorganic-organic derivatives before and after 10 d water treatment

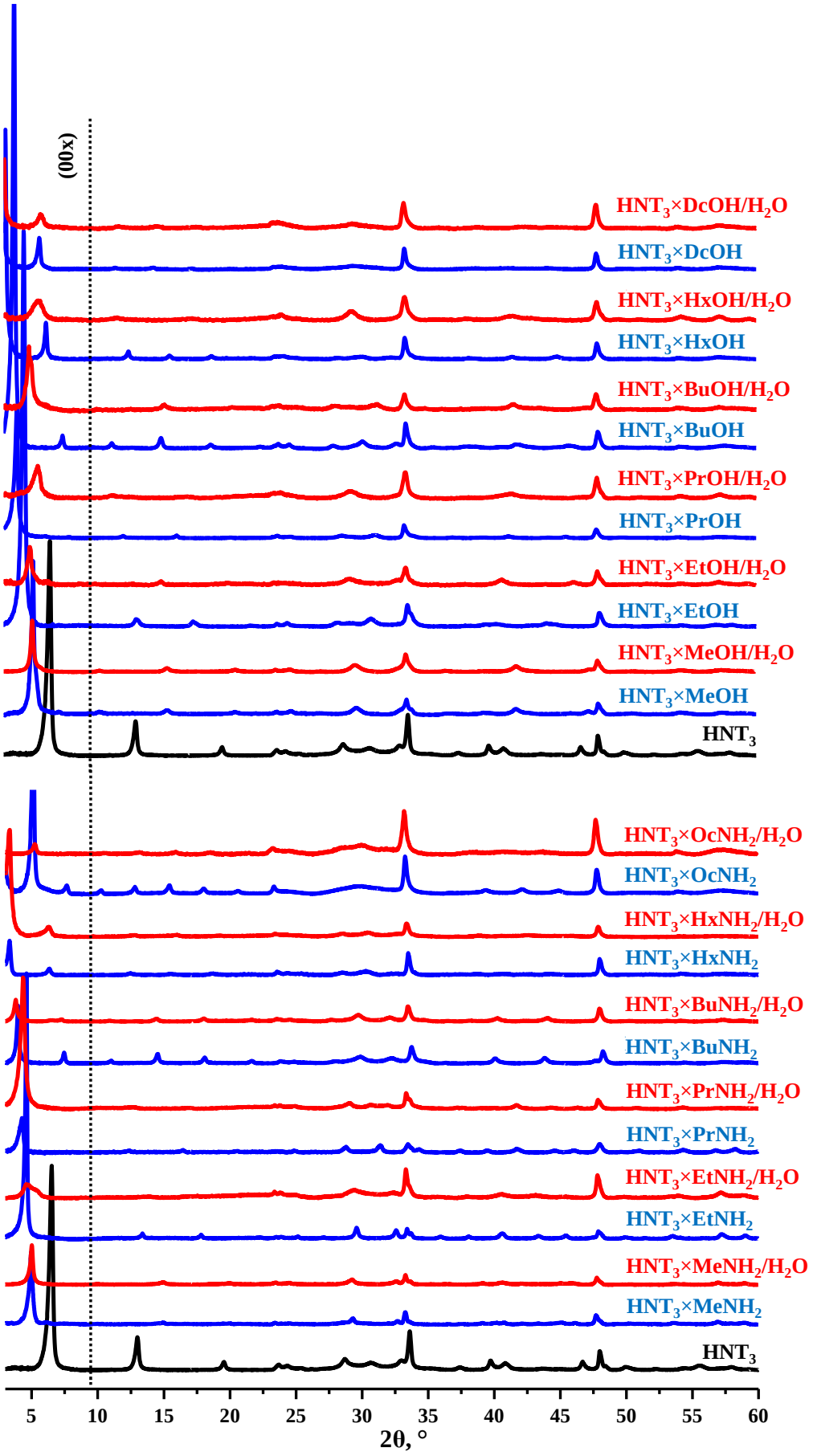

Supporting Information S9

Full kinetic curves of photocatalytic hydrogen generation over initial protonated titanates and their composites with Pt as a cocatalyst

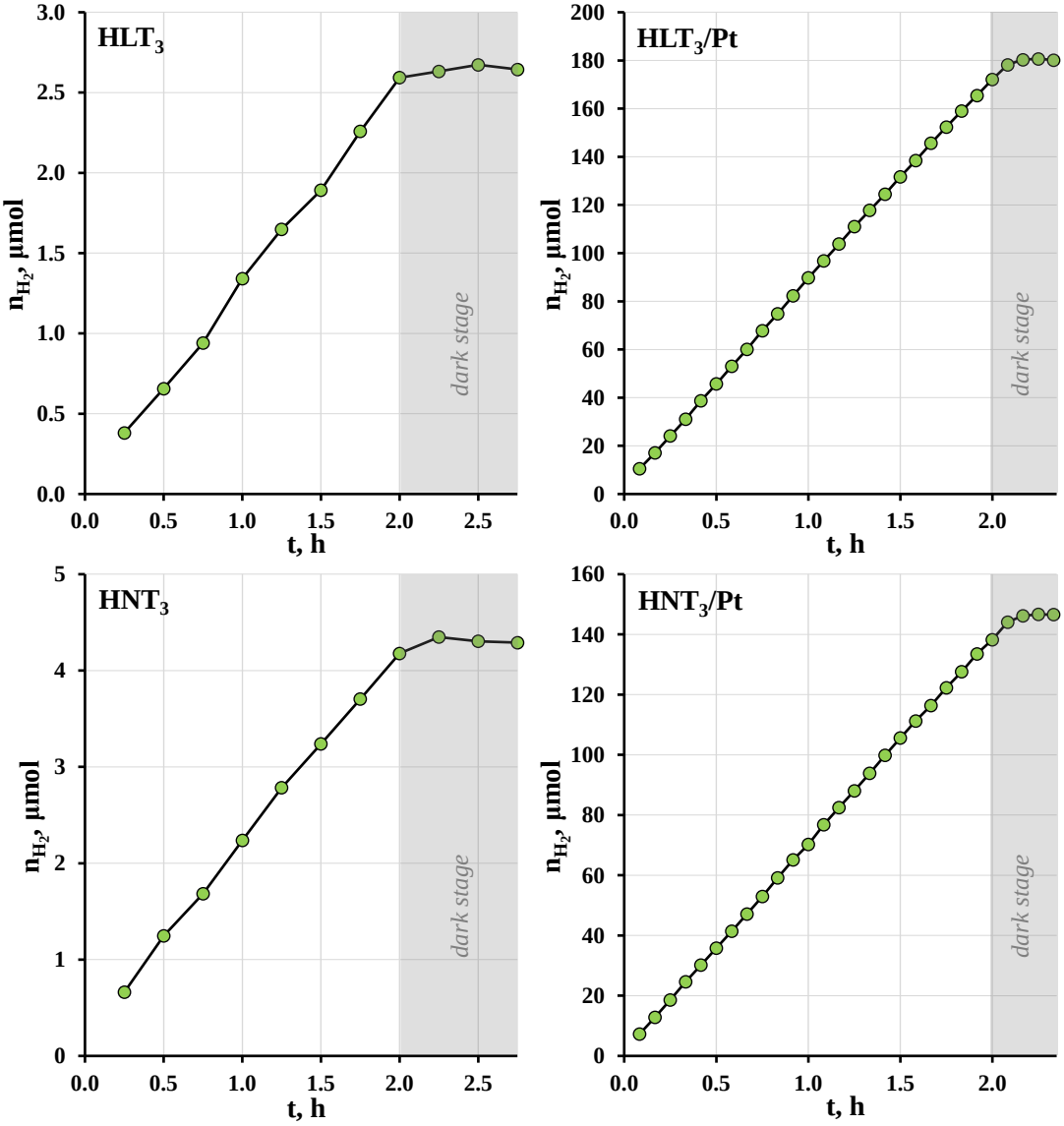

Supporting Information S10

Full kinetic curves of photocatalytic hydrogen generation over *n*-alkylamine derivatives and their composites with Pt as a cocatalyst

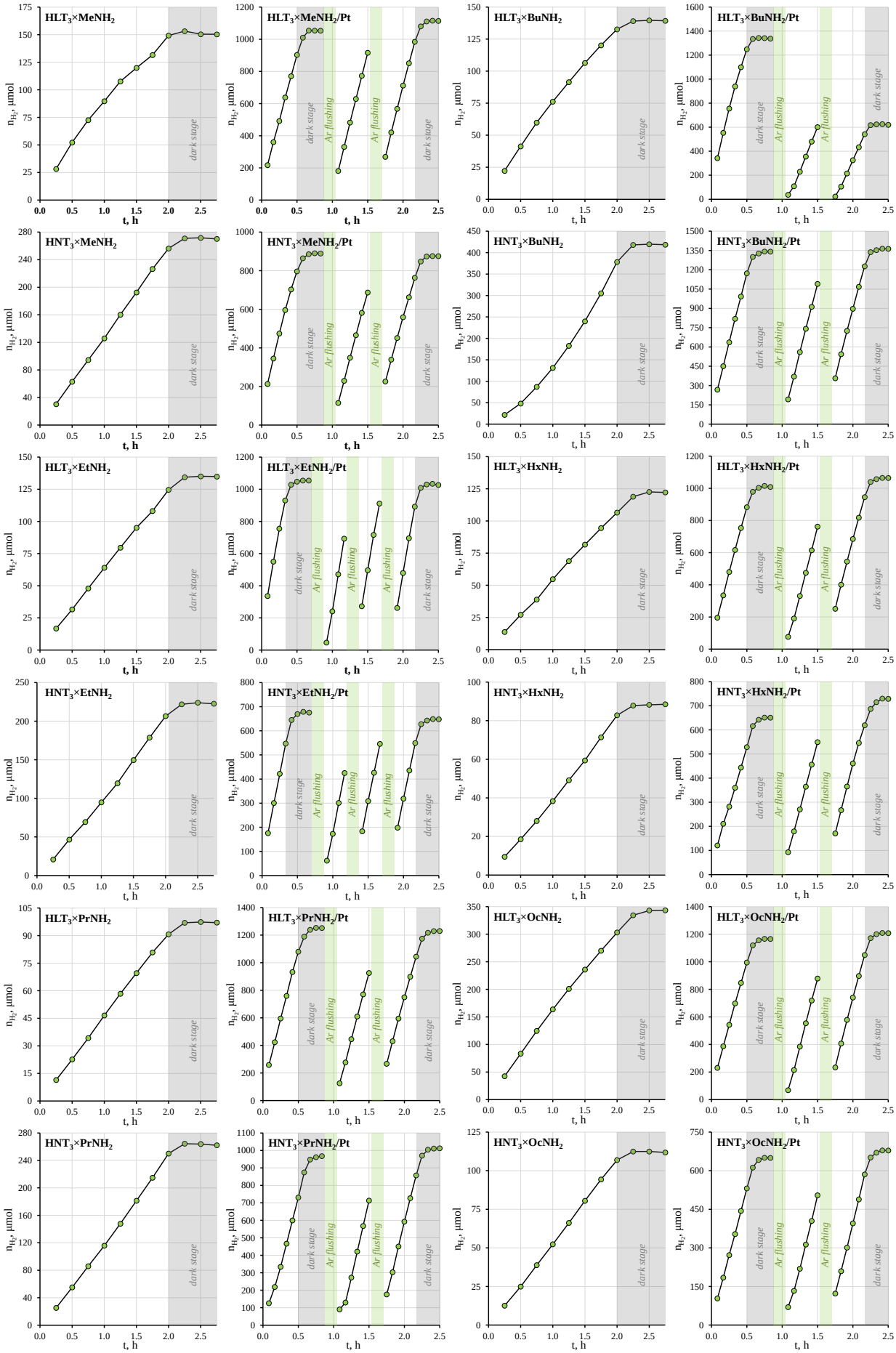

Supporting Information S11

Full kinetic curves of photocatalytic hydrogen generation over *n*-alkoxy derivatives and their composites with Pt as a cocatalyst

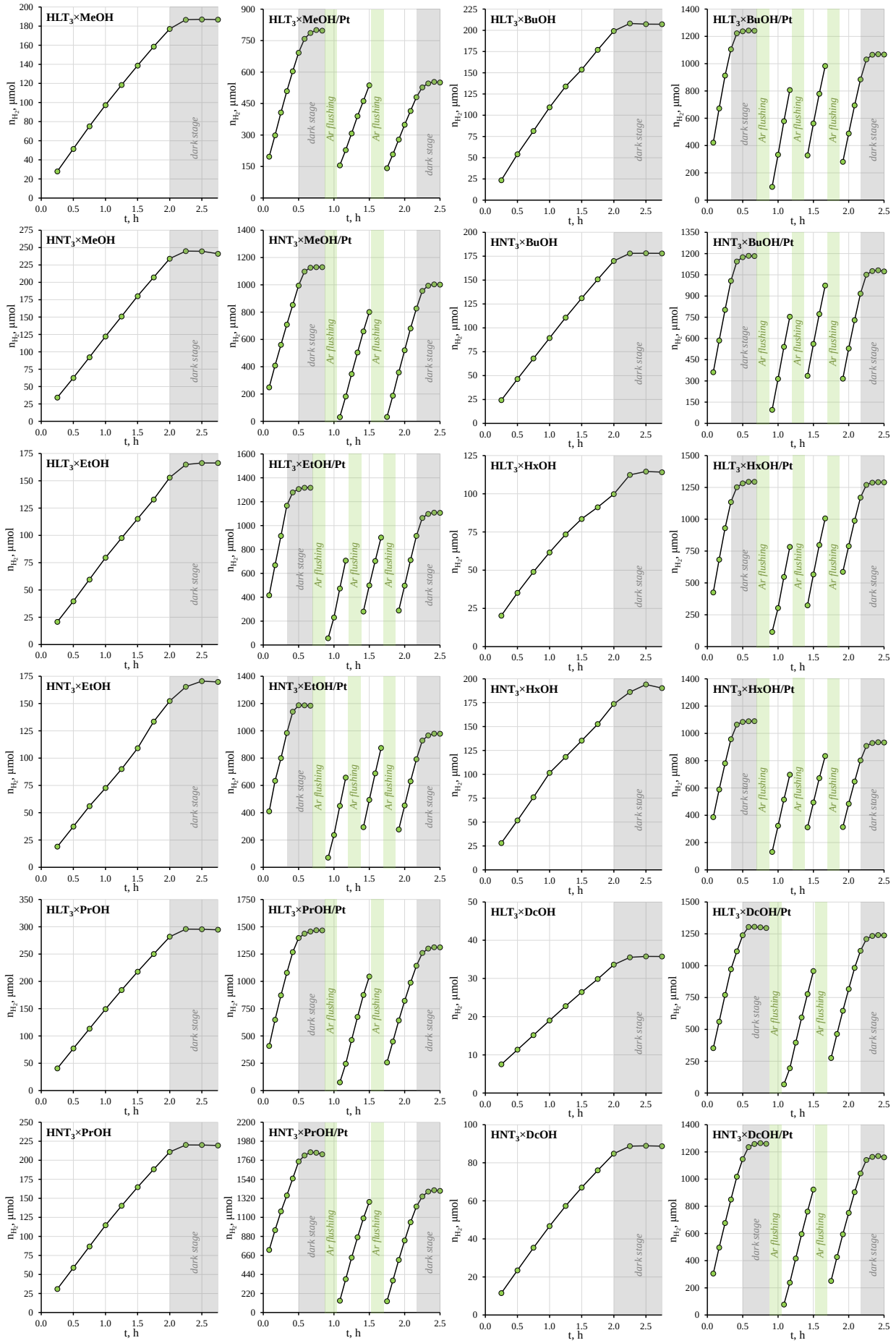

Supporting Information S12

Actual volume concentrations and pH values of reaction suspensions of La-containing samples

Photocatalyst	c_1, mg/l	c_2, mg/l	c_3, mg/l	pH_1	pH_2	pH_3
HLT_3	317	183	0.3	5.3	5.4	5.2
HLT_3/Pt	205	109	–	4.4	4.4	4.3
HLT_3×$MeNH_2$	327	109	0.3	7.5	5.3	5.1
HLT_3×$MeNH_2$/Pt	188	63.5	–	3.7	3.1	3.1
HLT_3×$EtNH_2$	497	454	0.6	8.1	7.2	6.7
HLT_3×$EtNH_2$/Pt	439	291	–	4.0	3.3	3.3
HLT_3×$PrNH_2$	331	325	0.8	7.9	7.5	7.5
HLT_3×$PrNH_2$/Pt	285	135	–	4.2	3.4	3.4
HLT_3×$BuNH_2$	345	344	0.7	8.5	6.9	7.2
HLT_3×$BuNH_2$/Pt	347	96.6	–	4.4	3.6	3.6
HLT_3×$HxNH_2$	307	301	0.7	8.6	7.7	7.7
HLT_3×$HxNH_2$/Pt	273	156	–	4.5	3.6	3.6
HLT_3×$OcNH_2$	354	20.2	0.5	8.7	5.8	5.6
HLT_3×$OcNH_2$/Pt	314	274	–	4.3	3.5	3.5
HLT_3×MeOH	269	240	0.6	4.2	3.7	3.7
HLT_3×MeOH/Pt	230	57.2	–	3.5	3.1	3.1
HLT_3×EtOH	190	171	0.0	5.1	4.4	4.3
HLT_3×EtOH/Pt	229	155	–	3.5	3.1	3.1
HLT_3×PrOH	242	174	0.4	5.0	3.8	3.7
HLT_3×PrOH/Pt	88.1	42.7	–	3.5	3.1	3.0
HLT_3×BuOH	180	139	0.3	5.0	4.1	4.1
HLT_3×BuOH/Pt	145	78.0	–	3.4	3.1	3.0
HLT_3×HxOH	144	108	0.2	4.9	4.8	4.6
HLT_3×HxOH/Pt	132	100	–	3.5	3.1	3.0
HLT_3×DcOH	81.3	61.6	0.2	4.8	4.8	4.7
HLT_3×DcOH/Pt	217	216	–	3.6	3.1	3.1

Supporting Information S13

Actual volume concentrations and pH values of reaction suspensions of Nd-containing samples

Photocatalyst	c_1, mg/l	c_2, mg/l	c_3, mg/l	pH_1	pH_2	pH_3
HNT_3	247	205	0.6	6.8	4.3	4.2
HNT_3/Pt	165	72.2	–	4.6	4.6	4.6
HNT_3×$MeNH_2$	309	120	0.6	7.4	4.0	4.0
HNT_3×$MeNH_2$/Pt	223	65.3	–	3.7	3.2	3.2
HNT_3×$EtNH_2$	491	239	0.4	7.8	4.8	4.7
HNT_3×$EtNH_2$/Pt	441	186	–	4.5	3.7	3.7
HNT_3×$PrNH_2$	331	72.5	0.5	8.3	5.0	4.9
HNT_3×$PrNH_2$/Pt	320	80.5	–	6.9	3.5	3.5
HNT_3×$BuNH_2$	441	93.0	0.8	8.2	5.0	4.9
HNT_3×$BuNH_2$/Pt	399	352	–	4.1	3.1	3.1
HNT_3×$HxNH_2$	301	240	1.3	8.4	7.4	7.5
HNT_3×$HxNH_2$/Pt	267	245	–	4.8	3.7	3.7
HNT_3×$OcNH_2$	322	72.8	0.3	7.5	6.9	6.6
HNT_3×$OcNH_2$/Pt	325	267	–	6.2	3.8	3.8
HNT_3×MeOH	226	168	0.9	4.6	4.0	3.9
HNT_3×MeOH/Pt	346	127	–	3.7	3.1	3.1
HNT_3×EtOH	220	153	0.7	4.9	4.4	4.5
HNT_3×EtOH/Pt	306	210	–	3.6	3.1	3.1
HNT_3×PrOH	271	136	0.3	4.8	4.4	4.3
HNT_3×PrOH/Pt	230	133	–	3.4	3.0	3.0
HNT_3×BuOH	161	125	0.5	4.9	4.5	4.4
HNT_3×BuOH/Pt	199	175	–	3.5	3.0	3.0
HNT_3×HxOH	177	146	0.7	4.9	4.5	4.4
HNT_3×HxOH/Pt	190	139	–	3.6	3.0	3.0
HNT_3×DcOH	181	109	0.4	5.1	4.7	4.6
HNT_3×DcOH/Pt	350	247	–	3.8	3.2	3.2

Supporting Information S14

Comparison of actual concentrations of samples in the reaction suspensions in the beginning and in the ending of the photocatalytic measurement

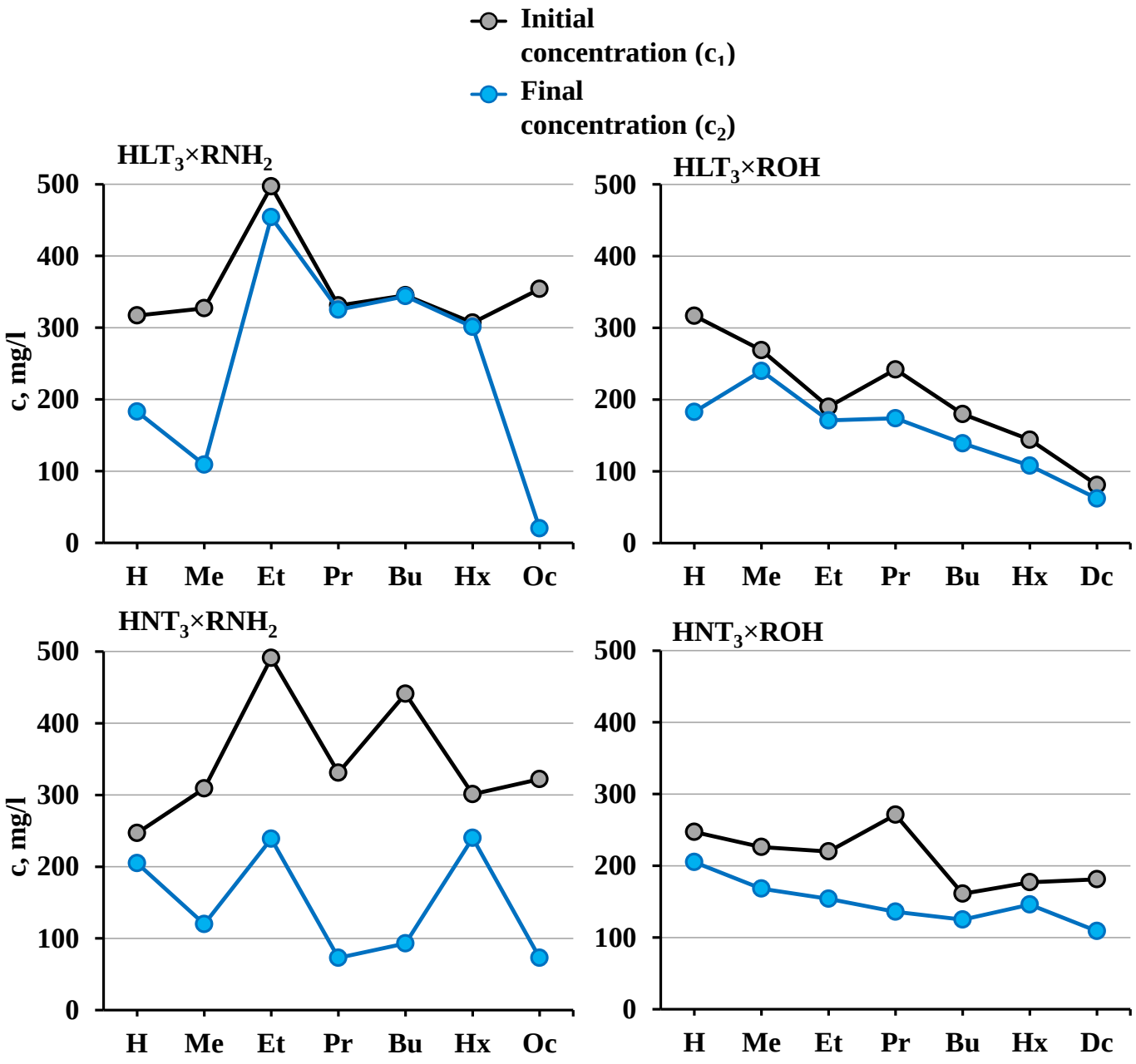

Supporting Information S15

XRD patterns of some inorganic-organic derivatives before and after photocatalytic (PC) experiments

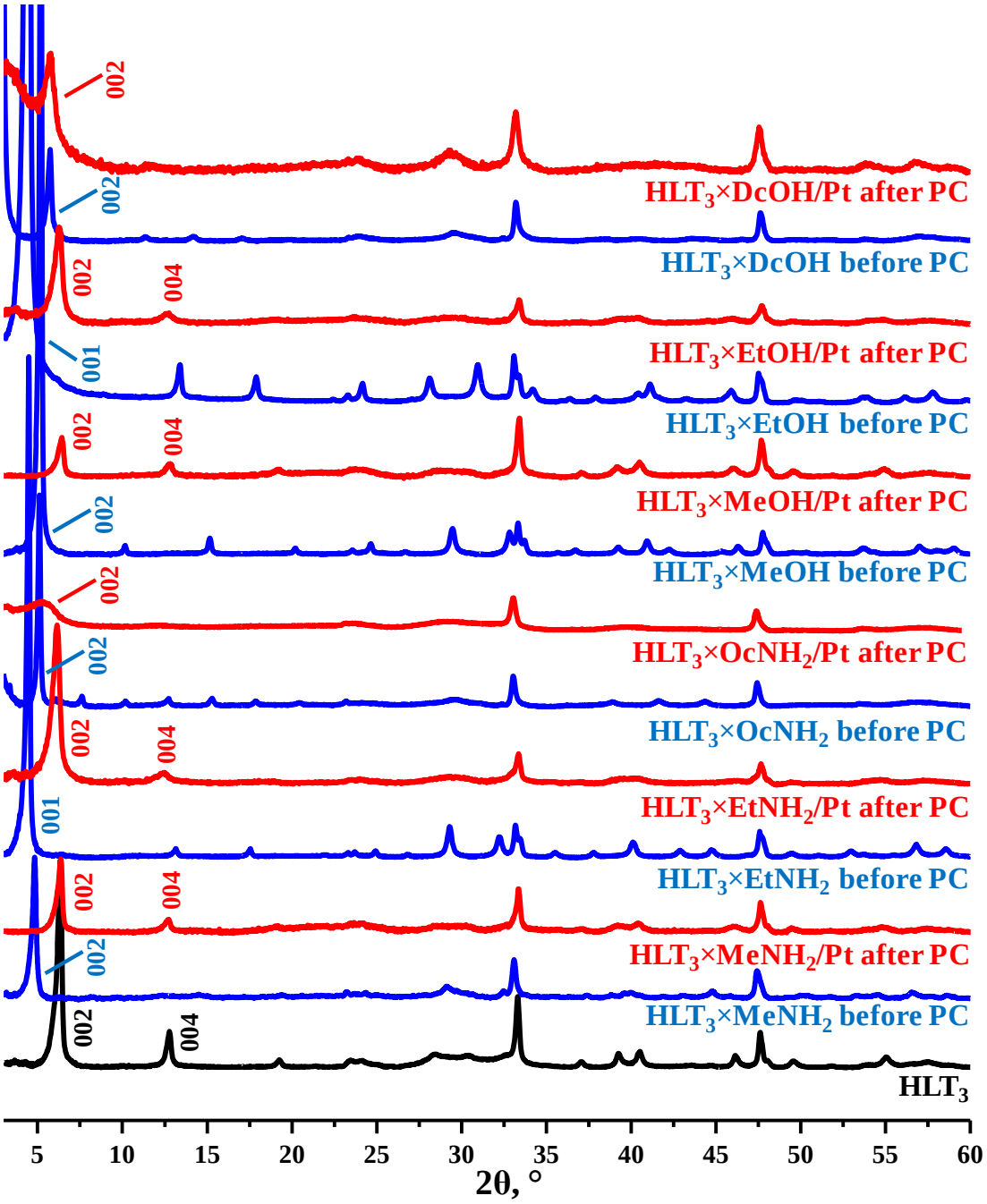

Supporting Information S16

Raman spectra of some inorganic-organic derivatives before and after photocatalytic (PC) experiments

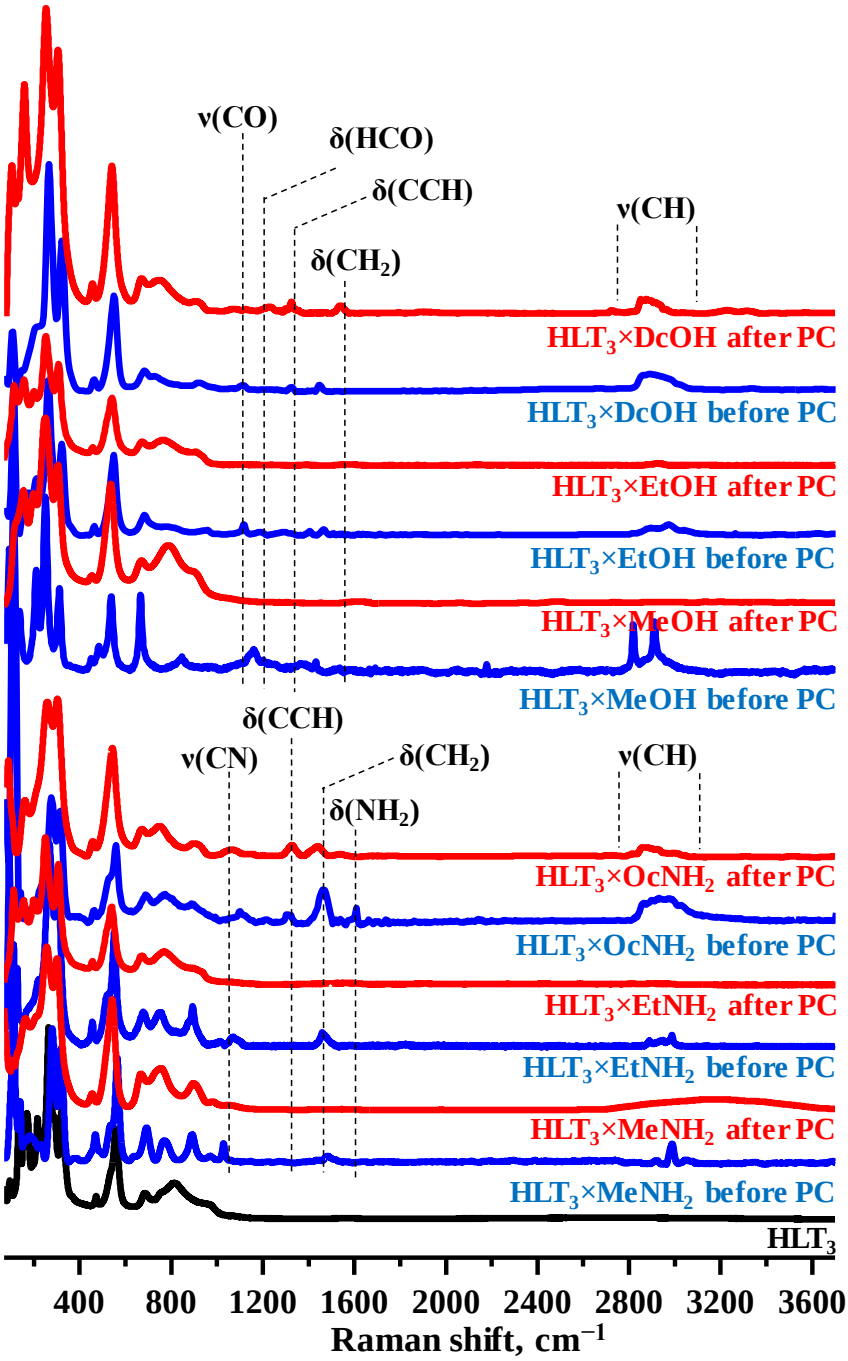

Supporting Information S17

TG curves of some inorganic-organic derivatives before and after photocatalytic (PC) experiments

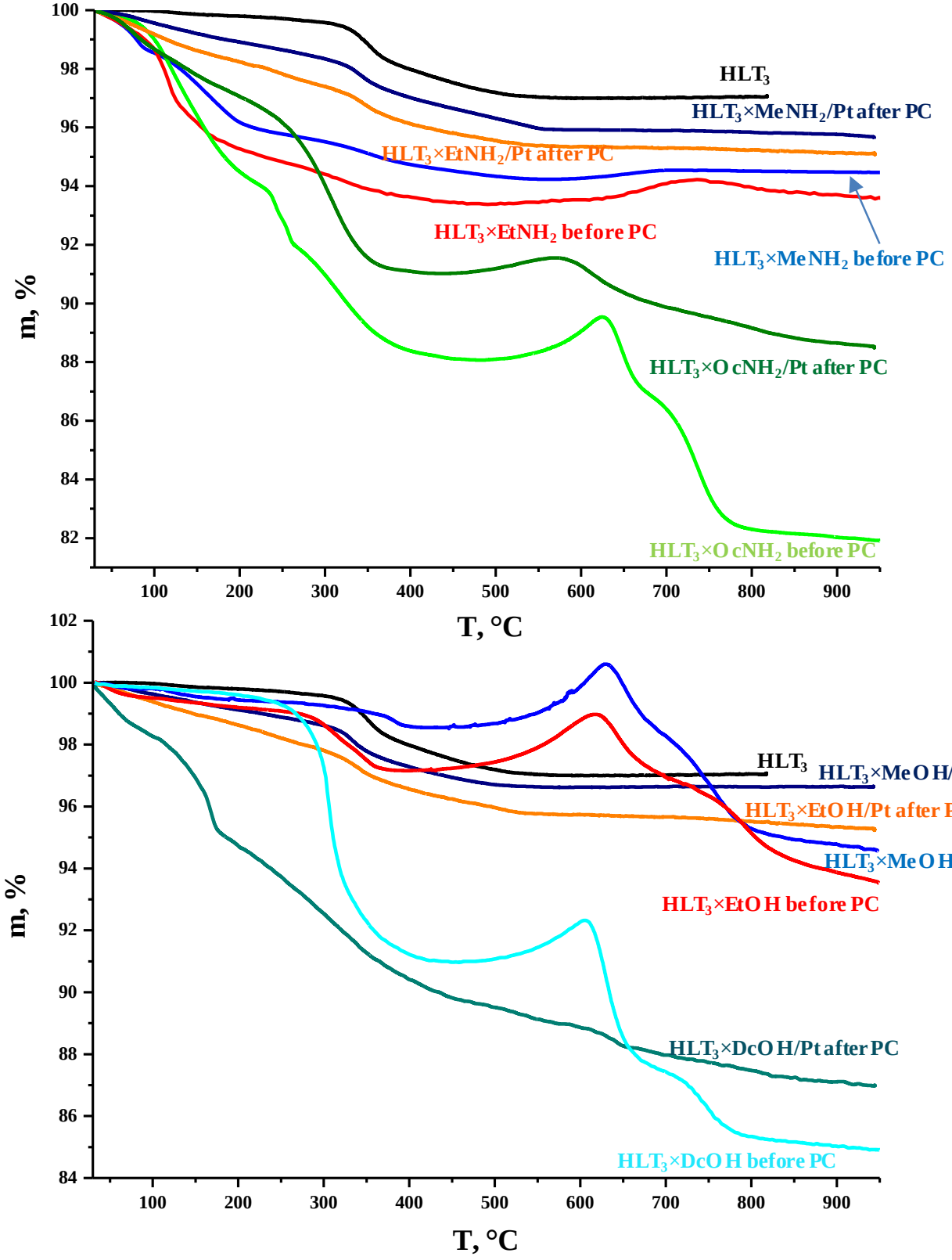

Supporting Information S18

SEM images of some inorganic-organic derivatives before and after photocatalytic (PC) experiments

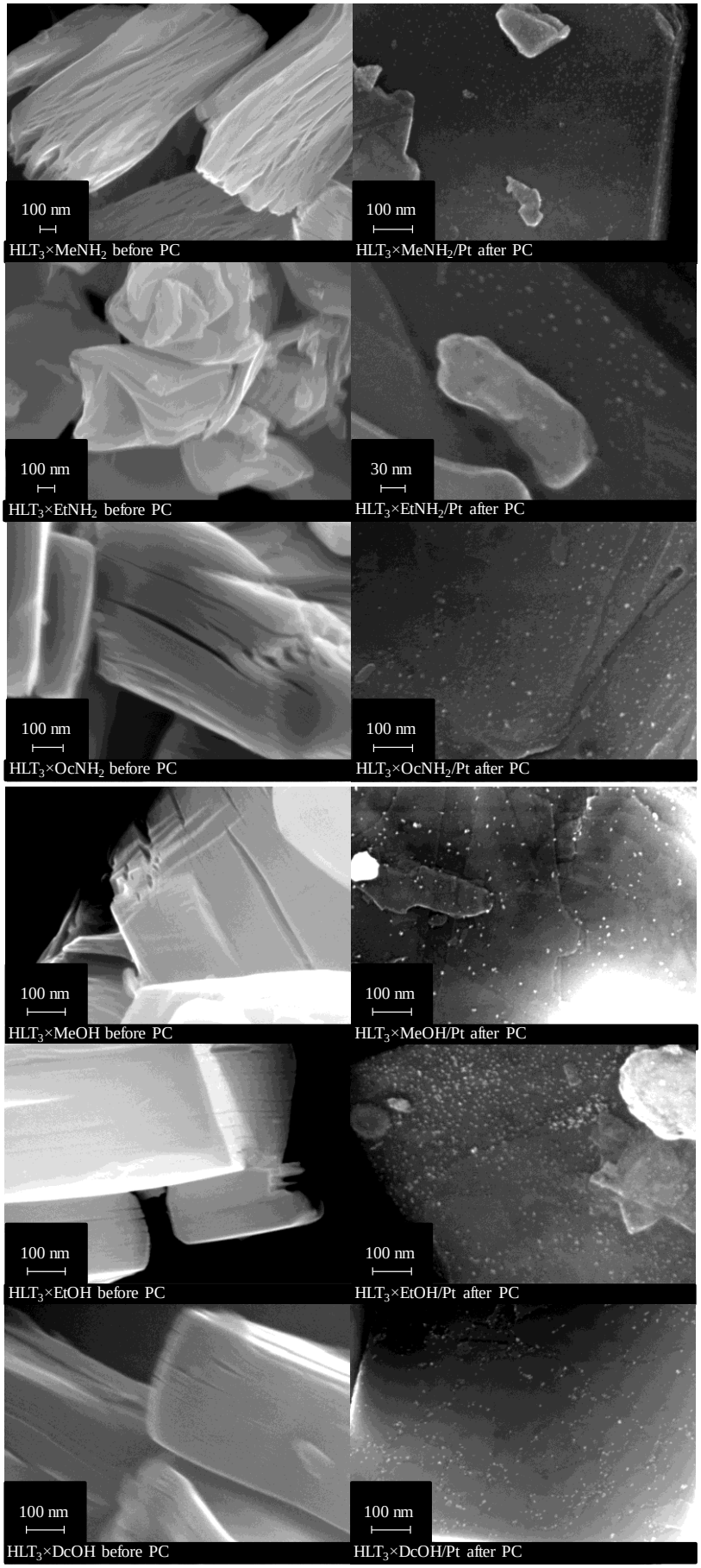

Supporting Information S19

Scheme of (a) photocatalytic setting and (b) reaction cell

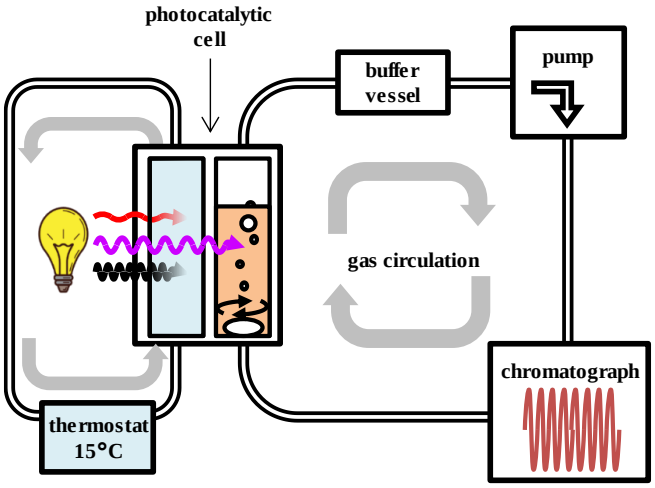

(a)

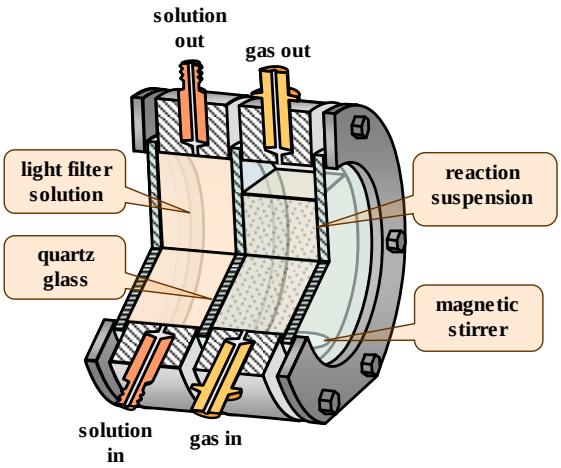

(b)

Supporting Information S20

Spectrophotometric calibrations for express measurement of reaction suspensions' concentrations

To prepare the calibration plot for suspensions of bulk non-exfoliated titanates for determination concentrations c_1 and c_2 during photocatalytic experiments, a hitch of each methylamine derivative $HLT_3 \times MeNH_2$ or $HNT_3 \times MeNH_2$, containing by calculation 0.03 g of the inorganic component (excluding intercalated water) was added to 60 ml of 1 mol. % methanol. Then the mixture was sonicated for 10 min in an Elmasonic S10H bath (60 W). Afterwards, the suspension obtained was used to build the spectrophotometric calibration dependence in coordinates optical density (A) – titanate concentration in mg/l (c). For this, a series of spectra with various suspension dilutions was recorded, analytical wavelength λ = 550 nm was selected and linear approximation of the experimental dependence $A_\lambda = A_\lambda$ (c) was found using the least-squares method (graphs a, b).

To prepare the calibration plot for suspensions of titanates exfoliated into nanolayers for determination concentration c_3 during photocatalytic experiments, a hitch of each methylamine derivative $HLT_3 \times MeNH_2$ or $HNT_3 \times MeNH_2$, containing by calculation 0.03 g of the inorganic component (excluding intercalated water) was placed into a glass tube with 30 ml of 0.004 M aqueous tetrabutylammonium hydroxide (TBAOH) and sonicated by a Hielscher UP200St homogenizer (200 W) at half power for 5 min. After shaking at room temperature for 24 h, the suspension was sonicated for 5 min again. Hereafter bulk non-exfoliated particles were separated via centrifuging at the separation factor F = 1000 for 1 h and concentration of the colloidal solution obtained was determined by ICP-AES after preliminary acid digestion. To obtain the calibration plot A – c (mg/l), a series of spectra with various suspension dilutions was recorded, analytical wavelength λ = 230 nm was selected and linear approximation of the experimental dependence $A_\lambda = A_\lambda$ (c) was found using the least-squares method (graphs c, d).